Performance of solar far-side active regions neural detection

E. G. Broock[1,2], T. Felipe[1,2], A. Asensio Ramos[1,2]
[1] Instituto de Astrofísica de Canarias; [2] Universidad de La Laguna

Far-side helioseismology is routinely used to compute the wave field on the Sun's hemisphere not facing the Earth using near-side helioseismic data. Active region predictions are then deduced from those wave fields due to the time-travel perturbation they induce on the waves. A detailed description of helioseismic holography can be found in Lindsey & Braun (2000a). These far-side predictions are crucial for improving Space Weather forecasting. Current techniques are limited to the detection of strong active regions due to the limiting signal-to-noise.

A neural network approach was developed to achieve better far-side active region predictions than standard helioseismic methods. We tested the network and compared its outputs with those of phase-sensitive helioseismic holography, finding that the network greatly improves the detections.

Data

Far-side seismic maps

We used maps obtained from the Joint Science Operation Center (JSOC) repository, at http://jsoc.stanford.edu/ajax/lookdata.html, computed using helioseismic holography from Doppler data obtained by the Helioseismic and Magnetic Imager (HMI) onboard the Solar Dynamics Observatory (SDO). The seismic maps are published in Carrington coordinates. Two kinds of phase-shift maps are published on the JSOC repository, one computed with 24 hours of Doppler data (used as network inputs) and the other computed using 5 days of data (used as standard approach inputs).

STEREO/SDO data

As proxies of active regions, we used STEREO/SDO 304 Å Carrington maps from the Solar Museum Server of NASA, found at https://solarmuse.jpl.nasa.gov/data/euvisdo_maps_carrington_12hr/304fits/ (Liewer et al, 2014).

Neural network:

FarNet (Felipe and Asensio 2019) is a fully convolutional neural network with a U-net architecture (Ronneberger et al. 2015). FarNet takes as input 11 consecutive phase-shift maps computed from HMI Doppler data using helioseismic holography. Each map is obtained from observations acquired during 24 hours and the temporal cadence between consecutive maps is 12 hours. Only a region of the seismic maps, centered on the central meridian of the far-side and ranging 120◦ in longitude and 144◦ in latitude, is given to the network as input.

The output of the neural network consists of a probability map with the same size as the input maps. The reliability of the detections are based on the integrated probability (P_i) of the output blobs, with units of deg^2. A threshold of P_i>100 has been taken as a real detection in previous works (Felipe and Asensio, 2019).

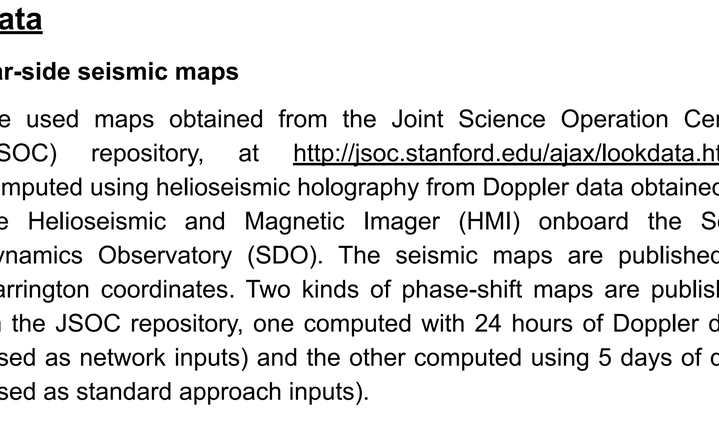

Fig. 1. Network Architecture.

Standard helioseismic method

The standard helioseismic method for far-side activity detection uses data from a surface region on the near-side of the Sun (pupil) to infer the properties of a region on the far-side (focal point). The presence of strong far-side active regions is routinely detected using Stanford's Strong-Active-Region Discriminator (SARD) on phase-shift maps processed with five days of HMI Doppler data. The method searches for regions where the negative phase-shift is greater than 0.085 rad (4s time-shift) and calculates their corresponding seismic strength (S), which is given by the integrated negative phase shift over the area of the region. A signal is classified as a far-side active region if the seismic strength (S) exceeds a threshold of 400 μHem rad (Liewer et al. 2017).

Comparison method

We studied the performance of both methods with data from April 2011 to May 2016. 2342 far-side active regions predictions were computed with each method. We compared the outputs of both methods with STEREO/SDO EUV images. EUV emission is linked with magnetic activity and has been used as an activity proxy by Liewer et al. 2017.

The predictions are computed using data from a range of dates (6 days in the case of the neural network and 5 in the case of the standard approach), which can lead to uncertainties on the position of the active regions on the predictions. We compared each prediction with a range of EUV images centered on the prediction date. We studied the comparisons of the outputs of both methods with 3, 7, and 11 STEREO/SDO Carrington images (24, 72 and 120 hours of data).

We computed activity masks from EUV images, using a date-dependent threshold for each image that was calibrated with HMI nearside magnetograms. Then, we compare the blobs of the outputs of both methods with the blobs on the generated activity masks that fell on the comparison range of said output. A detection was confirmed if there was a feature on one of the activity masks of the comparison range with a centroid within ±15º in longitude and ±5º in latitude from the centroid of the output blob at study. If the output blob had an area over 127 deg^2, superposition with features on activity masks was taken as a detection. This area was selected because it is the typical area of a Pi=100 region on the network outputs. If none of the criteria were met, the output blob was considered a false positive.

Results:

For S>400, the standard method detected 1334 active regions, with 52 false positives, a 3.75% of false positives. For Pi>113 and a false positive percentage of 3.74% (nearest to the standard method result for S>400), the network detected 1958 active regions. For the same percentage of false positives, the neural network can provide a 47% increase in the number of far-side active region detections confirmed by their extreme ultraviolet brightness.

	Detections	False Positives
SS $S > 400$	1334	52 (3.75%)
NN $P_i > 113$	1958	76 (3.74%)

Table 1. Detections, false positives and false positives percentage given by the standard method (first row) and for the neural network (second row), for regions with S>400 and P_i>113. P_i>113 gives the closest percentage of false positives to S>400, increasing the detections by 47%.

On figure 3 it can be noted how, for every range of study, when false positives tend to zero, the network returns more detections than the standard method. For the 24 hours study, for P_i>120, the network returns nearly zero false positives and close to 2000 detections, while for the standard method, for S>400, the method returns nearly zero false positives but less than 1500 detections.

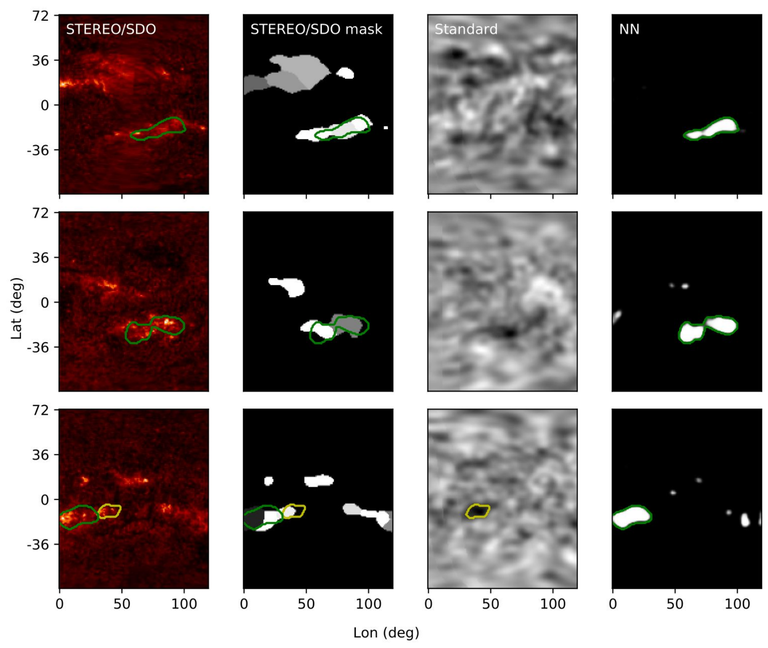

Fig. 2: *First column*: STEREO images and silhouettes of network detections with P_i>100 (green) and standard method detections with S>400 (yellow). *Second column*: EUV masks with same silhouettes. *Third column*: 5 days cumulative phase-shift maps with standard method silhouettes for S>400. *Fourth column*: network outputs with network silhouettes for P_i>100.

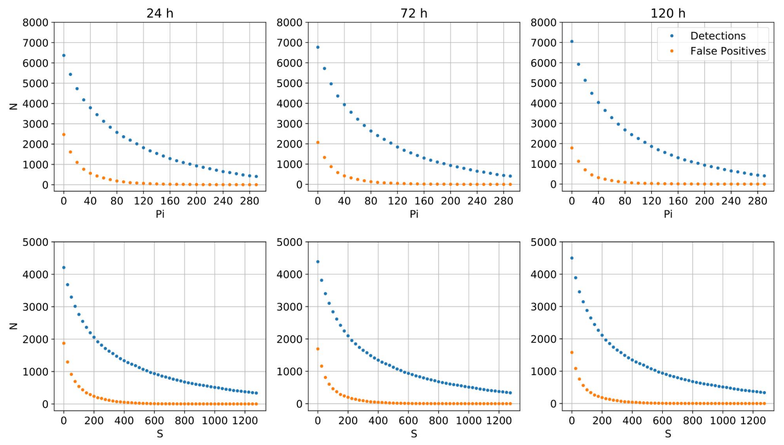

Fig. 3. Detections (blue dots) and false positives (orange dots) from FarNet (first row) and from the standard seismic method (second row) over the whole range of dates at study. Each dot corresponds to the detections with Pi or S over the X axis value. Each column represents the results of the comparison with 24 h (first column), 72 h (second column), and 120 h (third column) of STEREO data.

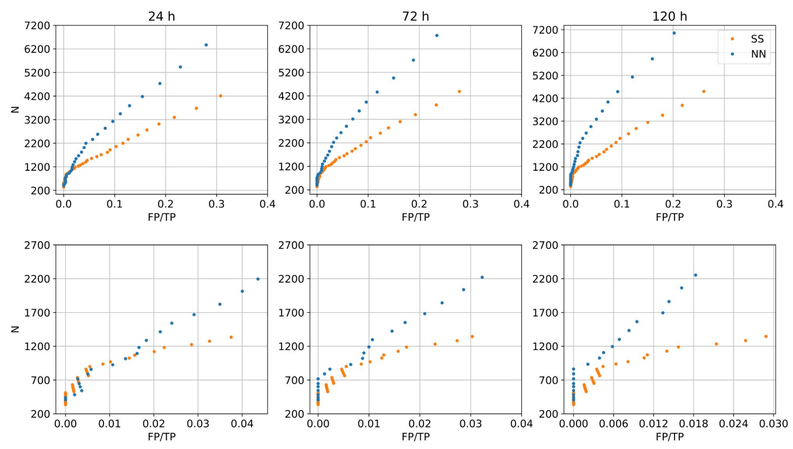

Fig. 4. Number of true detections from both methods as a function of the ratio of false positives to total positives. Second row shows a close-up look at the results from thresholds higher than *S* = 400 (standard seismic method) and *P*i = 100 (FarNet). Each column represents the results of the comparison with 24 h (first column), 72 h (second column), and 120 h (third column) of STEREO data.

References:

· Felipe, T. & Asensio Ramos, A. 2019, Astronomy & Astrophysics, 632, A82

· Liewer, P. C., González Hernández, I., Hall, J. R., Lindsey, C., & Lin, X. 2014, Sol. Phys., 289, 3617

· Liewer, P. C., Qiu, J., & Lindsey, C. 2017, Sol. Phys., 292, 146

· Lindsey, C. & Braun, D. C. 2000a, Sol. Phys., 192, 261

· Ronneberger, O., Fischer, P., & Brox, T. 2015, arXiv e-prints, arXiv:1505.04597